were successful (with the final result within 2 to 3% of the global minimum). With this degree of precision, the global minimum in all our test functions was "isolated" from local minima, so that the solution could always be refined to any desired accuracy by any local optimizer. We used the findminimum routine, a built-in local optimizer in Mathematica (Wolfram Research, Champaign, Illinois), which we believe to be a variant of the Newton-Raphson method.

Together with SA and GA, TS has been singled out as extremely promising for future practical applications (*19*). This work is a first step in applying the ideas and strategies of TS to continuous optimization. SA, GA, and TS are all based on a combination of combinatorial optimization and concepts from rather unlikely fields. Thus, SA is inspired by statistical physics and in essence amounts to a numerical simulation of the physical annealing of solids where, by slowly decreasing the temperature from the molten state, the system solidifies in a state of minimum energy. Genetic algorithm relies on the Darwinian principle of evolution: The algorithm cross-breeds trial solutions and allows only the "fittest" to survive after several iterations. Taboo search stems from the general tenets of intelligent problem-solving and is based on concepts from artificial intelligence.

Preliminary results for a standard set of test functions thus indicate that continuous TS is reliable and efficient, even more so than PRS and the multistart method. Taboo search reduces the amount of blind search that is characteristic of earlier techniques. The results obtained with TS compare favorably with those obtained with SA. The efficient optimization of the Hartman family of functions is particularly encouraging, given the great physical importance of the sums of Gaussian functions.

Our approach to continuous global optimization has several attractive features: (i) TS avoids entrapment in local minima and continues the search to give a near-optimal final solution; (ii) it is problem-independent and can be applied to a wide range of tasks; (iii) it does not require any information about the derivatives of the function to be minimized; (iv) it is very easy to implement and the entire procedure occupies only a few lines of code; and (v) it is conceptually much simpler than SA and GA. For instance, instead of using the metropolis algorithm, choosing a cooling program, and specifying an annealing schedule (the initial and final temperatures, temperature decrement, and the length of the Markov chain), the elementary version of TS (involving one taboo list and an aspiration function) requires only empirical control parameters: the size of the taboo list and a parameter defining the partition of the solution space.

All the same, we are aware that no stochastic method can be guaranteed to solve the multiple minima problem in a finite number of steps, and any method may require long computing times. Also, just like SA, TS is a heuristic method and thus requires theoretical justification. Its appeal is largely intuitive, and little theoretical analysis is available. Making the method more effective is thus necessarily a matter of numerical experimentation.

The algorithm allows vectorization, and parallel computing could reduce computing time, especially in problems of a higher dimension. The method is also open to further improvement. The introduction of concepts such as long-term memory, diversification of search, and strategic oscillation could reduce the number of iterations without improvement. More sophisticated approaches to the neighborhood structure [different partitioning of the solution space or the use of techniques described (*6*)] may also be developed.

REFERENCES

1. L. C. W. Dixon and G. P. Szego, *Towards Global Optimization* (North-Holland, New York, 1975), vol. 1.
2. ———, *Towards Global Optimization* (North-Holland, New York, 1978), vol. 2.
3. S. Kirkpatrick, C. D. Gelatt Jr., M. P. Vecchi, *Science* **220**, 671 (1983).
4. W. H. Press, S. A. Teukolsky, W. T. Vetterling, B. P. Flannery, *Numerical Recipes in C: The Art of Scientific Computing* (Cambridge Univ. Press, Cambridge, 1992).
5. P. M. Pardalos and J. B. Rosen, *Constrained Global Optimization: Algorithms and Applications* (Springer-Verlag, Berlin, 1987).
6. A. Törn and A. Žilniskas, *Global Optimization* (Springer-Verlag, Berlin, 1989).
7. C. Floudas and P. M. Pardalos, *Recent Advances in Global Optimization* (Princeton Univ. Press, Princeton, NJ, 1991).
8. K. D. Gibson and H. A. Scherega, in *Structure and Expression: From Proteins to Ribosomes*, M. H. Sarma and R. H. Sarma, Eds. (Adenine Press, Guilderland, NY, 1988), vol. 1, pp. 69–81.
9. R. Fletcher, *Practical Methods of Optimization* (Wiley, New York, 1980), vol. 1.
10. ———, *ibid.*, vol. 2.
11. P. J. M. van Laarhoven and E. H. L. Aarts, *Simulated Annealing: Theory and Applications* (Kluwer, Dordrecht, 1987).
12. D. E. Goldberg, *Genetic Algorithms in Search, Optimization, and Machine Learning* (Addison Wesley, Reading, MA, 1989).
13. F. Glover, *ORSA J. Comput.* **1**, 190 (1989).
14. ———, *ibid.* **2**, 4 (1990).
15. A. Hertz and D. de Werra, *Computing* **39**, 345 (1987).
16. C. Frieden, A. Hertz, D. de Werra, *ibid.* **42**, 35 (1989).
17. A. Törn and A. Žilniskas, *Global Optimization* (Springer-Verlag, Berlin, 1989), p. 185.
18. R. S. Anderssen, in *Optimisation*, R. S. Anderssen, L. S. Jennings, D. M. Ryan, Eds. (Univ. of Queensland Press, St. Lucia, Australia, 1972), pp. 27–34.
19. Committee on the Next Decade of Operations Research (Condor), *Oper. Res.* **36** (1988).
20. A. Dekkers and E. Aarts, *Math. Program.* **50**, 367 (1991).

13 July 1994; accepted 23 November 1994

Simulation of Recent Global Temperature Trends

Nicholas E. Graham

Observations show that global average tropospheric temperatures have been rising during the past century, with the most recent portion of record showing a sharp rise since the mid-1970s. This study shows that the most recent portion of the global temperature record (1970 to 1992) can be closely reproduced by atmospheric models forced only with observed ocean surface temperatures. In agreement with a diverse suite of controversial observational evidence from the past 40 years, the upward trend in simulated tropospheric temperatures is caused by an enhancement of the tropical hydrologic cycle driven by increasing tropical ocean temperatures. Although it is possible that the observed behavior is due to natural climate variability, there is disquieting similarity between these model results, observed climate trends in recent decades, and the early expressions of the climatic response to increased atmospheric carbon dioxide in numerical simulations.

Observations indicate that global average surface air temperatures have been rising during the past century (*1, 2*). Whether this trend is real and if so what processes are responsible are questions that have been the subject of much discussion, particularly because increased tropospheric temperature is one of the most consistent results from simulations of the effects of increasing concentrations of CO_2 and other greenhouse gases (*3*). The recent portion of the global tropospheric temperature record is characterized by a sharp rise beginning during the mid-1970s, with the signal of the El Niño–Southern Oscillation (ENSO) superimposed on the lower frequency changes (*4*). The results presented here show that this most recent portion of global air temperature record can be simulated closely by atmospheric general circulation models (GCMs) forced only with observed global ocean temperatures. Analyses show that both the ENSO time scale changes and the

Climate Research Division, Scripps Institution of Oceanography, La Jolla, CA 92093, USA.

lower frequency upward trend in model global tropospheric temperatures are due principally to fluctuations in tropical precipitation. These fluctuations in tropical precipitation, the manifestation of variability in the model hydrologic cycle, have been driven in turn by changes in the prescribed sea surface temperatures (SSTs).

These findings are significant from a variety of perspectives. First, the agreement between the simulated and observed global average land surface air temperature adds further support to the validity of the recent observed record (*5, 6*). Second, the results demonstrate that numerical models can play a useful role in monitoring and diagnosing the physical processes responsible for climate change. Most important, the model results corroborate and link a diverse (and generally unaccepted) set of observational findings suggesting that the recent upward trend in global temperature has been caused by an enhancement of the tropical hydrologic cycle driven by increasing tropical ocean temperatures (*4, 7–9*).

An important early result concerning the latter point was the demonstration of a close relation between fluctuations in tropical Pacific SSTs and changes in global surface air temperatures (*4, 5, 10*). This relation suggests that global tropospheric temperatures are modulated by changes in the tropical hydrologic cycle; that is, warmer tropical SSTs cause increased evaporation and increased precipitation, thereby heating the atmosphere through the release of latent heat. Other observational studies have attempted to directly detect changes in the activity of the tropical hydrologic cycle. Although such studies necessarily rely on historical data that suffer from real and potential problems of various kinds (*11, 12*), the results have been generally consistent in suggesting an increasingly active tropical hydrologic cycle during the past few decades (*7–9*), particularly since the mid-1970s. These findings include evidence for increases in evaporation (*5, 13*), tropospheric moisture content (*14–16*), and precipitation over the tropical oceans and the tropical Pacific in particular (*17–19*). These changes, and other notable aspects of recent climate variability, have apparently been driven by increasing tropical SSTs (*7, 8, 17, 19, 20*).

In a few cases, numerical model results have been used to help corroborate the observed changes in the tropical hydrologic cycle. In one of these, Gaffen and Barnett (*21*) showed that a numerical model (ECHAM1) driven with observed global SSTs reproduced the sharp (10 to 20%) rise in tropospheric moisture content (as inferred from radiosonde measurements) over the tropics during the mid-1970s (*14, 15*). Other studies have used model results to

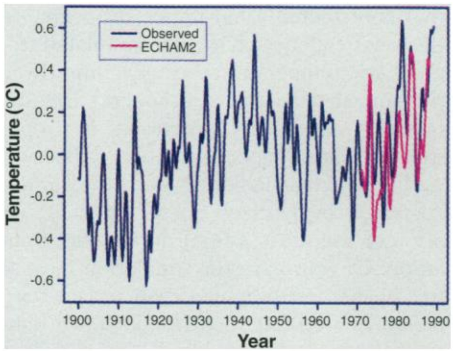

Fig. 1. Observed global average land surface air temperatures (*22*) for the period 1900 to 1989, and the corresponding results from the ECHAM2 GLBL simulation, 1970 to 1988.

support the idea that this sharp climate shift was a result of changes in the tropical hydrologic cycle (*17, 19, 22*).

A final point relating to the significance of the findings presented here is that numerical simulations of the effects of increased atmospheric CO_2 show that a trend toward an enhanced tropical hydrologic cycle is a consistent and highly detectable signature of the early phases of greenhouse warming (*3*). Given the observational evidence for such a trend and the corroborating evidence from numerical simulations presented here, this point is of some concern.

Four observational data sets are used in the analyses presented here. Global surface air temperature data come from two gridded data sets. The first of these, described by Jones *et al.* (*23*), covers the period 1851 through 1992 and was compiled by careful inspection and compositing of the records from thousands of land observing stations. These data are supplied on a 5° latitude by 10° longitude grid. The second of these data sets, constructed by Ropelewski and Halpert (*24*) using similar quality control procedures, covers the period 1970 to 1992 on a 2.5° by 2.5° grid. Comparison of these two temperature records during this period shows excellent agreement over the continental tropics and Northern Hemisphere (correlations above 0.95), with poorer agreement over the Southern Hemisphere. In all cases, the surface air temperature data presented here are from continents and very large islands (for example, Greenland) only; data from oceanic areas and smaller islands have been excluded.

The observed land precipitation data used in these analyses, described by Eischeid and co-workers (*25*), covers the period 1851 through 1991 and is supplied on a 4° latitude by 5° longitude grid. Observations of satellite-derived outgoing long-wavelength radiation (OLR) are used as a proxy for oceanic tropical precipitation (*26*). These data, originally 5-day averages on a 2° by 2° grid covering the period 1974 to 1987 (with some gaps), were processed into monthly averages on the ECHAM2 model's 5.5° by 5.5° grid. Actual and potential problems with the OLR data have been documented (*27*) but have minimal impact on the results presented here. Furthermore, the findings based on OLR have been corroborated with other data (*17, 18*).

Simulated data from three atmospheric models are used in the analyses presented here. Two of these are versions of the climate model evolving at the Max Planck Institute of Meteorology at the University of Hamburg, denoted ECHAM2 and ECHAM3 (*28*). The models differ in parameterizations of physical processes and in their spatial resolutions of about 5° and 2.5° (spectral truncations T21 and T42), respectively.

Most of the results presented here are from a 19-year simulation with the ECHAM2 model in which observed SSTs were prescribed globally (designated the GLBL simulation). Also mentioned are results from two other simulations with the ECHAM2 model (*9, 17*). In one of these, observed SSTs were prescribed equatorward of approximately 30° latitude, with climatological SSTs elsewhere. In the other, observed SSTs were prescribed poleward of approximately 30° latitude, with climatological SSTs elsewhere (designated the EXTROP simulation). The ECHAM3 results come from one simulation covering the period 1970 to 1978 and the average of five simulations covering the period 1979 to 1992. Observed global SSTs were prescribed in each of these latter simulations, with different atmospheric initial conditions. Results are also shown from the GCM developed by the Coupled Model Project at the National Meteorological Center (NMC) (*29*). This model has vertical and horizontal resolution similar to that of the ECHAM3 model but uses different physical parameterizations. The data presented from this model are the average of nine simulations covering the period 1982 to 1993. Aside from SST, there were no changes in prescribed boundary conditions, atmospheric composition, or the solar constant during any of these simulations.

Figure 1 shows the smoothed (*30*) record of observed global average land surface air temperature over the period 1900 to 1989 [data of Jones *et al.* (*1*)]. In the observed record, the most distinctive features are a relatively rapid rise in temperature between 1920 and 1940, a slow decrease from 1940 until the mid-1970s, followed by another period of rapid temperature increase. Also shown in Fig. 1 are the results from the ECHAM2 GLBL simulation. The model closely reproduces the trend toward increasing tropospheric temperatures since the mid-1970s.

Figure 2 shows the smoothed record of observed global surface temperature data [data of Ropelewski and Halpert (*24*)] and the results from the ECHAM2 GLBL, ECHAM2 EXTROP, ECHAM3, and NMC simulations for the period after 1970. There is clear agreement between the observations and the model results for the simulations with global SSTs (*31*), with each record showing the association with ENSO activity noted by Newell and Weare (*10*), Pan and Oort (*5*), and Angell (*4*) and the trend toward warmer tropospheric temperatures since the mid-1970s (*1, 2, 4*). In contrast, the results from the ECHAM2 EXTROP simulation show little agreement with the observations, indicating that the model-data agreement in global land surface air temperature in the other simulations is due to the effects of tropical SSTs. Other comparisons (*9*) demonstrate that the ECHAM2 simulation forced with tropical SSTs shows a trend toward warmer global temperatures after the mid-1970s (*31*).

In light of the model-data agreement demonstrated in Figs. 1 and 2, it is of interest to consider how changes in tropical SSTs were communicated to the model atmosphere and how the model atmosphere responded. The temporal evolution of the dominant components of the model atmospheric heat budget from the ECHAM2 GLBL simulation (Fig. 3) shows that variability in the simulated atmospheric heat budget was dominated by changes in latent heat flux (that is, precipitation), which shows swings of ± 2 W m^{-2} in the global average during the simulation. A relation between the simulated latent heat flux and ENSO variability is also apparent, with peaks associated with the increased organized convection over the tropical Pacific during the 1972, 1982 to 1983, and 1986 to 1987 warm episodes. From the perspective of long-term change, the record shows a trend for increasing values since the mid-1970s with a total change in simulated global latent heating between 1970 and 1988 of about 1 W m^{-2}, about 1.5% of the global mean. Also demonstrated in Fig. 3 is that OLR was the dominant term in the model tropospheric heat budget acting to counter the effects of the increased latent heating, and the inverse relation between those two flux terms is apparent. However, the fluctuations in OLR are not as large as those in latent flux, and to first order it is this difference that leads the increase in tropospheric temperatures after the mid-1970s. Model OLR increased (recall that increased OLR represents a loss of energy from the atmosphere) by about 0.7 W m^{-2} (about 0.3% of the global average) between 1970 and 1988.

The other term in the model heat budget that contributed to an important degree to the low-frequency changes in simulated tropospheric temperature was upwelling (from the surface into the atmosphere) thermal radiation. Because of increases in tropospheric water vapor content, global upwelling thermal radiation from the surface decreased by perhaps 0.2 W m^{-2} (about 0.3% of the mean value) during the simulation. Of course, in the simulation most of this heat is lost because ocean surface temperatures are prescribed (land surface temperatures are calculated by the model). In a coupled system, however, this heat would be absorbed by the ocean and would thus contribute to further warming. In comparison with the three dominant flux terms described above, changes in sensible heating and solar absorption had little effect on the low-frequency temperature changes (*32*).

Even if only qualitatively correct, these results have important implications. They suggest that at time scales of years to decades the changes in global average surface air temperature observed during the 1970s and 1980s were driven almost entirely by changes in tropical SSTs. The variability in SST was communicated to the atmosphere through changes in tropical precipitation and evaporation. This is essentially the same suite of changes inferred by Pan and Oort (*5*) and Flohn *et al.* (*7, 8*) on the basis of observations.

The spatial structure of the changes in SST during the mid-1970s is evident in a map of the difference between the average surface temperatures for 1971 to 1976 and the means for 1977 to 1982 (*33, 34*) (Fig. 4A). One of the most apparent features is a wedge-shaped region in the Pacific where SSTs increased by 0.6° to 0.8°C. This region extends westward from the apex on the equator near the date line to the west coasts of North and South America near 40° latitude (of particular interest is the fact that this pattern of anomalous SSTs has recurred frequently in recent years). Warmer water is also found over much of the Indian and subtropical North Atlantic oceans. Cooler water is found over the mid-latitude North (*17, 19, 35*) and South Pacific and the subtropical South Atlantic. The distribution of differences in simulated evaporation for the two sets of 6 years (*9*) resembles that for SST (Fig. 4A), showing a trend toward increased evaporation over warmer water. The largest increases are in the central tropical Pacific, where values reach up to about 15 W m^{-2} (about 0.5 mm day^{-1}).

The energy transferred from the ocean to the atmosphere by evaporation is expressed as atmospheric heating when condensation and precipitation occur. Figure 4B shows the 6-year differences in precipitation from the ECHAM2 simulation, expressed in watts per square meter (*36*). The largest increases in simulated precipitation (30 to 45 W m^{-2}) are found in a small region of the equatorial Pacific between 170°E and 180°, with an area of more modest increases extending toward the east-southeast. Increased precipitation is also depicted over large areas of the central and eastern subtropical Pacific and much of the Indian Ocean. Large decreases in simulated precipitation are depicted over Indonesia, eastern South America, and eastern Africa. Decreased precipitation is also indicated over

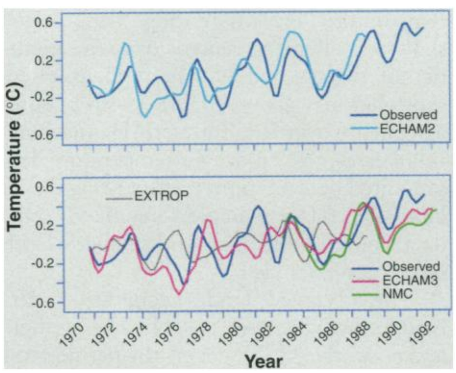

Fig. 2. Observed global average land surface air temperatures (*23*) for the period 1970 to 1991 (both panels) from the ECHAM2 GLBL simulation (upper) and the ECHAM3, NMC, and ECHAM2 EXTROP simulations (lower).

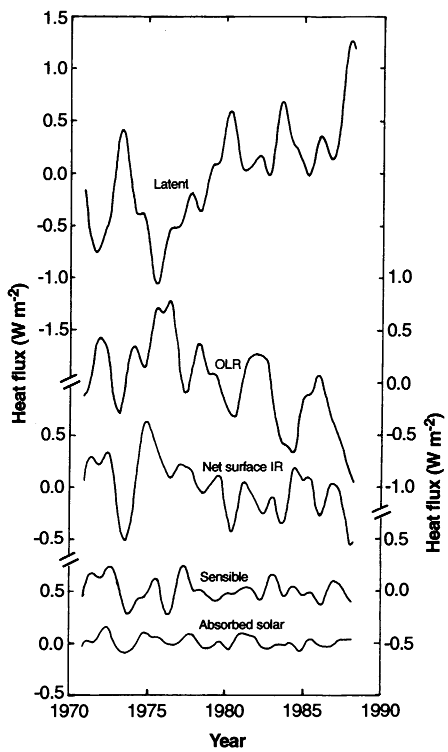

Fig. 3. Components of the atmospheric heat budget from the ECHAM2 GLBL simulation. Positive (negative) values indicate more (less) heat released into the atmosphere.

much of China, India, and northern South America and flanks the equatorial rainfall maximum in the western tropical Pacific.

For direct comparison with the changes in simulated precipitation (Fig. 4B), Fig. 4C shows corresponding 6-year differences in precipitation from the data of Eischeid *et al.* (*25*). There are several points of agreement between the observed and simulated fields, but one of the most obvious is that both show drier conditions during the latter set of 6 years over many tropical land regions, including much of tropical eastern Asia and northern South America. Over the central equatorial Pacific, the coverage provided by this data is quite limited, but the available data are consistent with the simulated pattern in suggesting an area of large increases in precipitation extending east-southeast from near the date line, with decreased precipitation to the north.

Because variability in simulated precipitation over the west-central tropical Pacific contributed importantly to the changes in simulated global temperatures (Figs. 3 and 4B), it is critical to establish that such major increases in precipitation can be documented in the observed record. Evidence suggesting that such an increase in precipitation did occur comes from studies of the major climate shift over the Pacific during the mid-1970s (*17*, *19*). These studies show that this climate shift coincided with sharp increases in satellite-inferred precipitation (OLR) in the west-central equatorial Pacific. Using statistical and numerical model results, the authors of these studies conclude that the large-scale circulation changes that accompanied the climate shift resulted from the changes in precipitation over the tropical Pacific, which in turn were forced by the increased SSTs in that region (Fig. 4A). Figure 5 depicts differences between the average OLR values for January 1977 to June 1982 and the averages for June 1974 (the first month that OLR data are available) to December 1976 (over the tropical oceans, lower OLR values are typically indicative of higher precipitation; this is especially true of the area in question). Also depicted are the differences in simulated precipitation for the same period, with data only from those months when

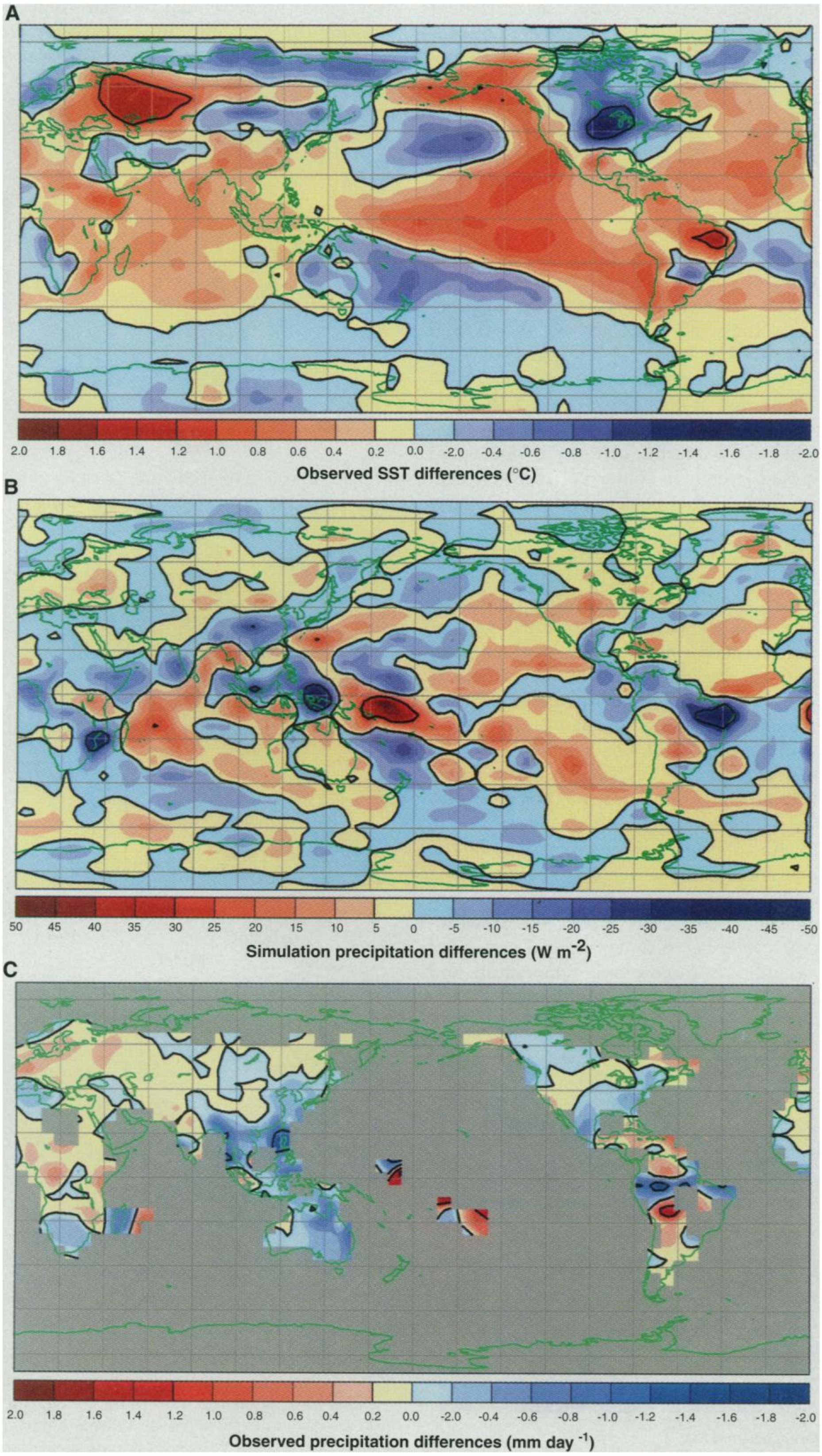

Fig. 4. Differences in 6-year means for 1977 to 1982 less 1971 to 1976 for (**A**) observed SST, (**B**) simulated precipitation, and (**C**) observed precipitation. Simulated data are from the ECHAM2 GLBL simulation; red (blue) denotes increased (decreased) flow of heat into the atmosphere.

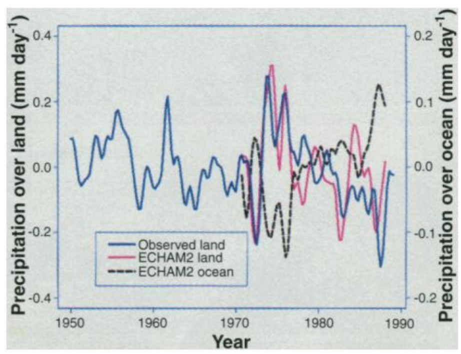

Fig. 5. Observed and simulated precipitation from tropical continental regions (left scale) and simulated precipitation over tropical oceans (right scale); simulated data come from the ECHAM2 GLBL simulation.

OLR data were available. The two maps agree in indicating large increases in precipitation near the date line in the equatorial Pacific during the years after 1976; the changes in simulated precipitation in this region of about 2 mm day^{-1} represent about 20% of the simulated annual mean in that region. Recently, additional evidence supporting the reality of the increases in precipitation in the tropical Pacific near the date line has become available (*18*). This evidence, in the form of analyses of historical precipitation data from the western and central tropical Pacific, shows magnitudes and spatial patterns that are quite consistent with those seen in the simulated precipitation data in Figs. 4B and 5.

As pointed out earlier, a notable point of agreement between observed and simulated changes in precipitation (Fig. 4, B and C) is the indication of decreasing precipitation over extensive regions of the continental tropics after the mid-1970s. Figure 6 shows the simulated and observed records of average precipitation over tropical continental regions (that is, regions that the ECHAM2 model considers to be land). The records show clear agreement (*37*) in indicating large fluctuations in tropical land precipitation during the early 1970s followed by a sharp decline after 1976. This decline of about 0.3 mm day^{-1} represents a substantial 11% of the average (2.7 mm day^{-1}). This out-of-phase relation between continental and oceanic precipitation is also found in the ECHAM3 model results.

A further comparison between the observed and simulated indices of the tropical hydrologic cycle is presented in Fig. 7, which shows observed [after Flohn *et al.* (*8*), see also (*13*)] and simulated (ECHAM2 GLBL) records of the near-surface vertical gradient in specific humidity (δq) (*38*) over the global near-equatorial oceans between 1970 and 1988 (*39*). The qualitative agreement between the observed and simulated records is apparent, with each record showing fluctuations associated with ENSO activity and a lower frequency upward trend in δq of about 4% between 1970 and 1988. This agreement between the simulated and observed records of δq is important because the results presented above indicate that during recent decades global average precipitation and temperature have been controlled largely by tropical evaporation. This suggests that estimates of observed tropical evaporation based on historical ship observations might provide a diagnostic for past changes in the global tropospheric heat budget. Such estimates of observed oceanic evaporation are often calculated as proportional to the product of the wind speed and δq. When such estimates are made for the past 40 years, they show a large upward trend in tropical evaporation of about 5% (about 5 W m^{-2}) per decade since 1950 (*8, 13*). Approximately 60% of this increase is due to an upward trend in observed marine wind speeds that other evidence strongly suggests is artificial (*12*). The model results are in agreement with this latter evidence and show a slight decrease in tropical marine surface wind speeds during the simulation (*40*); thus, the trends in simulated evaporation (and precipitation and global temperature) are due almost entirely to changes in δq. If actual tropical marine evaporation is estimated assuming no change in surface wind speeds (*8*), the simulated and observed records of marine evaporation agree closely in indicating an upward trend of about 2% per decade over the period 1970 to 1988, much as suggested by the records of δq depicted in Fig. 7.

As a final comparison between observed and simulated indices of the tropical hydrologic cycle, Fig. 8 shows vertical profiles of variability in tropospheric temperature and moisture content from the western Pacific over the period between 1974 and 1988 (*16, 41*). These distributions were calculated by partitioning the temporal specific humidity record at each level into a linear trend and the detrended residual, then expressing the variability in each component as a standard deviation. The two profiles of

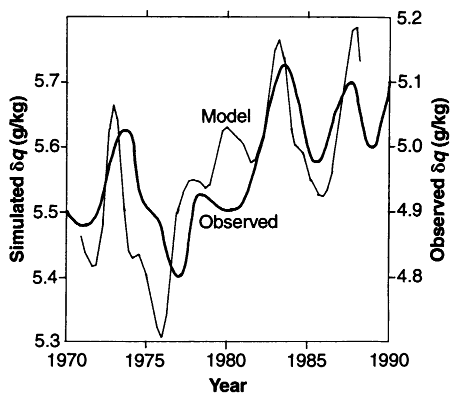

Fig. 7. Simulated δq (ECHAM2 GLBL) and that based on observations [after Flohn *et al.* (*8*)].

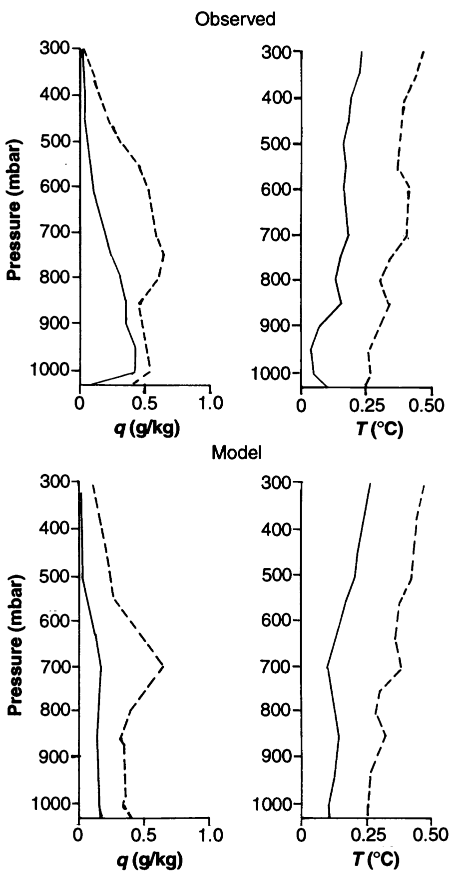

Fig. 8. Simulated (ECHAM2 GLBL) and observed [after Gutzler (*16*)] vertical profiles of standard deviations variability in tropospheric temperature (σ_T) and specific humidity (σ_q) over the western tropical Pacific. As in (*16*), the solid curves show standard deviations due to the linear trend, and the dashed curves show the standard deviations due to all other variability except the annual cycle.

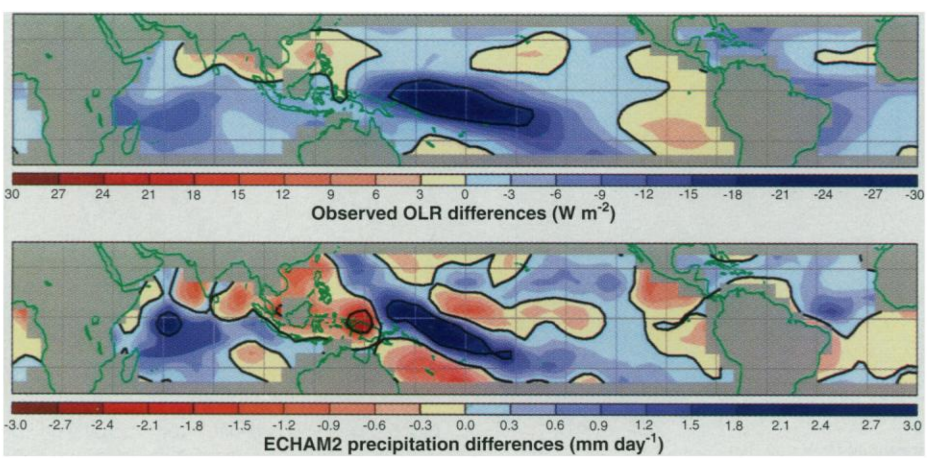

Fig. 6. Differences in observed OLR (upper) and simulated precipitation (ECHAM2 GLBL simulation) (lower) for the period January 1977 through June 1982 less those from June 1974 through December 1976; only those months when observed OLR data are available have been used in both.

observed temperature variability (representing high- and low-frequency variability, respectively) have similar vertical structures, with each showing a steady increase in altitude (*42*). In contrast, the moisture variability profiles show quite different structures. The profile for the linear trend shows the maximum value at 1000 mbar and then decreases with height (*43*), and the higher frequency variability shows a peak in variability near 750 mbar.

The lower panels in Fig. 8 show the corresponding profiles of moisture and temperature variability from the ECHAM2 GLBL simulation. The temperature variability profiles are quite similar to those estimated from the observations. The moisture variability profiles agree with the observed distributions in that the profiles for high- and low-frequency variability are quite different, with the former showing a peak near 700 mbar. The profile for the linear trend shows values 30 to 50% of those observed but correctly decreases with height from near the surface.

These results show that the recent upward trends in global tropospheric temperature have been caused principally by an increasingly active tropical hydrologic cycle driven by increasing tropical ocean temperatures. This finding emphasizes the importance of the tropical hydrologic cycle as a fundamental index of global climate and climate change (*44*). A key question regarding the genesis of recent climate changes is how warmer-than-normal SSTs have been maintained over much of the global tropics since the mid-1970s during which evaporative fluxes have apparently increased by about 5%. It is troubling that the suite of observed and simulated changes suggesting an enhanced tropical hydrologic cycle are similar in important respects to the early manifestations of the climatic response to increasing concentrations of greenhouse gases (*3, 7, 9, 20*). Of course, the results presented here are not inconsistent with the possibility that the observed trends in the hydrologic cycle are simply the result of natural variability. Nevertheless, the similarity between recent observations of climate change and the early responses seen in simulations of greenhouse warming counsels caution in dismissing both as spurious.

REFERENCES AND NOTES

1. P. D. Jones, T. M. Wigley, P. B. Wright, *Nature* **322**, 430 (1986).
2. J. Hansen and S. Lebedeff, *J. Geophys. Res.* **92**, 13345 (1987).
3. M. E. Schlesinger, *Clim. Dyn.* **1**, 35 (1986); C. A. Wilson and J. F. Mitchell, *J. Geophys. Res.* **92**, 13315 (1987); J. Hansen *et al.*, *ibid.* **93**, 9341 (1988); J. G. Mitchell, in *Greenhouse-Gas–Induced Climate Change: A Critical Appraisal of Simulations and Observations*, M. E. Schlesinger, Ed. (Elsevier, New York, 1991), pp. 49–62; G. A. Meehl, W. M. Washington, T. Karl, *Clim. Dyn.* **8**, 117 (1993).
4. J. K. Angell, *Geophys. Res. Lett.* **17**, 1097 (1990).
5. Y. H. Pan and A. H. Oort, *Mon. Weather Rev.* **111**, 1244 (1983); see also J. K. Angell and J. Korshover, *J. Appl. Meteorol.* **20**, 1105 (1981).
6. G. Kukla, G. J. Gavin, T. R. Karl, *J. Appl. Meteorol.* **25**, 1265 (1986); J. K. Angell, *J. Clim.* **1**, 1296 (1988); P. D. Jones, P. M. Kelly, C. M. Goodess, T. Karl, *ibid.* **2**, 285 (1989); R. W. Spencer and J. R. Christy, *Science* **247**, 1558 (1990); *J. Clim.* **5**, 847 (1992); *ibid.*, p. 858.
7. H. Flohn, A. Kapala, H. R. Knoche, H. Mächel, *Clim. Dyn.* **4**, 237 (1990).
8. ———, *Meteorol. Z.* **1**, 122 (1992).
9. N. E. Graham, *SIO Tech. Rep. 94-25* (Scripps Institution of Oceanography, La Jolla, CA, 1994).
10. R. E. Newell and B. C. Weare, *Nature* **262**, 40 (1976); *Science* **194**, 1413 (1976).
11. J. F. Saur, *J. Appl. Meteorol.* **2**, 417 (1963); S. Tabata, *ibid.* **17**, 374 (1978); T. P. Barnett, *Mon. Weather Rev.* **112**, 303 (1984); C. S. Ramage, *J. Clim. Appl. Meteorol.* **23**, 187 (1984).
12. C. S. Ramage, *J. Clim. Appl. Meteorol.* **26**, 187 (1985); E. S. Postmentier, M. A. Cane, S. E. Zebiak, *J. Clim.* **2**, 731 (1989); V. J. Cardone, J. G. Greenwood, M. A. Cane, *ibid.* **3**, 113 (1990).
13. H. Flohn and A. Kapala, *Nature* **338**, 244 (1989).
14. A. P. Hense, P. Krahe, H. Flohn, *Meteorol. Atmos. Phys.* **38**, 215 (1988).
15. D. J. Gaffen, T. P. Barnett, W. P. Elliot, *J. Clim.* **4**, 989 (1991).
16. D. S. Gutzler, *Geophys. Res. Lett.* **19**, 1595 (1992).
17. N. E. Graham, *Preprints Fifth Conference on Climate Variations* (American Meteorological Society, Boston, MA, 1991), p. 109; *Clim. Dyn.* **10**, 135 (1994); ———, T. P. Barnett, R. Wilde, M. Ponater, S. Schubert, *J. Clim.* **7**, 1416 (1994).
18. M. Morrissey (private communication) has recently documented large upward trends in observed island rainfall in the central and western tropical Pacific since the early 1970s.
19. T. Nitta and S. Yamada, *J. Meteorol. Soc. Jpn.* **67**, 375 (1989).
20. A. Kumar, A. Leetmaa, M. Ji, *Science* **266**, 632 (1994).
21. D. J. Gaffen and T. P. Barnett, *J. Geophys. Res.* **97**, 2775 (1992).
22. R. A. Kerr, *Science* **255**, 1508 (1992); *ibid.* **266**, 544 (1994).
23. P. D. Jones *et al.*, "A Grid Point Surface Air Temperature Data Set for the Northern Hemisphere, 1951–1984," *Tech. Rep. TR022* (U.S. Dept. of Energy, Carbon Dioxide Research Division, Washington, DC, 1985).
24. C. F. Ropelewski and M. S. Halpert, *Mon. Weather Rev.* **114**, 2352 (1986).
25. J. K. Eischeid, H. G. Diaz, R. S. Bradley, P. D. Jones, "A Comprehensive Precipitation Data Set for Global Land Areas," *Tech. Rep. TR051* (U.S. Dept. of Energy, Carbon Dioxide Research Division, Washington, DC, 1991); R. S. Bradley *et al.*, *Science* **237**, 171 (1987).
26. P. A. Arkin, thesis, Univ. of Maryland (1984), p. 223–224; *Trop. Ocean Atmos. Newsl.* **17**, 5 (1983); M. L. Morrissey, *Mon. Weather Rev.* **114**, 931 (1986); C. E. Motell and B. C. Weare, *J. Clim. Appl. Meteorol.* **26**, 1436 (1987).
27. M. Chelliah and P. A. Arkin, *J. Clim.* **5**, 372 (1992); S. Gadgil, A. Guruprasad, J. Srinivasan, *ibid.*, p. 867.
28. H. von Storch, Ed., *Climate Simulations with the ECMWF T21 Model in Hamburg* (Large Scale Atmospheric Modelling Report 4, Meteorologisches Institut der Universitat Hamburg, Hamburg, Germany, 1988); E. K. Roeckner *et al.*, *Simulation of the Present-Day Climate with the ECHAM Model: Impact of Model Physics and Resolution* (Report 93, Max Planck Institüt für Meteorologie, Hamburg, Germany, 1992).
29. M. Ji, A. Kumar, A. Leetmaa, *Tellus A* **46**, 398 (1994).
30. The records shown have been smoothed with a cosine filter with a half-width of three seasons, giving a 0.1 power response at five seasons.
31. The correlations between the observed and simulated global land surface temperature records in Fig. 2: ECHAM2 GLBL (0.63, 0.69 with the model leading by one season), ECHAM3 (0.64), NMC (0.54, 0.58 with the model leading by one season), and ECHAM2 EXTROP (−0.02). For the ECHAM2 simulation with tropical SSTs only, the correlation is 0.51.
32. Integration of the fluxes of energy into the model atmosphere shows that the result obtained by using only OLR, latent flux, and upwelling thermal radiation gives nearly the same result as that obtained when solar absorption and sensible heat are included as well.
33. Recall that in the ECHAM2 model, the ocean temperatures are prescribed, but land temperatures are calculated by a surface energy balance model.
34. These two sets of years were selected because they lie on either side of the sharp changes noted in many climate variables during the mid-1970s.
35. E. L. Venrick, J. A. McGowan, D. R. Cayan, L. T. Hayward, *Science* **238**, 70 (1987); K. E. Trenberth, *Bull. Am. Meteorol. Soc.* **71**, 998 (1990); A. J. Miller *et al.*, *Clim. Dyn.* **9**, 287 (1994).
36. Divide the precipitation in watts per square meter by 28.9 to obtain the equivalent value in millimeters per day.
37. The correlation between the simulated and observed land precipitation records is 0.83.
38. Marine evaporation estimates are generally made using the "bulk aerodynamic formula" in which the evaporation rate E is given by $E = c_E U (\delta q)$ where c_E is a turbulent exchange coefficient, U is the wind speed at measurement height, and $\delta q = (q_s - q_a)$, where q_s is the saturation specific humidity at the water temperature and q_a is the specific humidity at measurement height.
39. Flohn *et al.* (*8*) used the global tropical oceans from 10°S to 14°N; the model data come from 11.2°S to 11.2°N.
40. A latitude-height cross section of the linear trends in model wind speeds shows slight (less than −0.2 m s^{-1} per decade) decreases throughout the troposphere in the tropics, with increases of the same order over much of the mid-latitude Northern Hemisphere. Larger increasing trends (up to 1.2 m s^{-1} per decade) are found in the upper troposphere over the mid-latitudes in the Southern Hemisphere.
41. Gutzler (*16*) averaged data from four radiosonde stations located between 6° and 8°N and 134° and 172°E over the period 1974 to 1988. The model data come from the region 6°S to 6°N and 143° to 172°E and are for the period 1970 to 1988.
42. The trends in temperature are approximately 0.1°, 0.4°, and 0.5°C per decade at 1000, 700, and 300 mbar, respectively.
43. In terms of percentage of the mean values, the observed trends represent changes of about 5, 7, and 16% per decade at 1000, 700, and 300 mbar, respectively.
44. In recent experiments (N. E. Graham and T. Barnett, unpublished results), a GCM was forced with observed SSTs for the period 1900 to 1990. The results show that the model reproduces important aspects of the observed global temperature record during the century.

45. Special thanks to T. Crowley, whose idea it was to compare the observed and simulated air temperature records, and to D. Cayan, W. Collins, T. Karl, V. Ramanathan, N. Schneider, and R. Somerville, whose insight and knowledge were indispensable in interpreting these results. Thanks as well to T. Barnett, S. Chen, H. Diaz, J. Eischeid, K. Georgakakos, S. Hartley, M. Latif, A. Leetmaa, M. Morrissey, and J. Roads for assistance, interest, ideas, and encouragement. Most of the ECHAM model simulations were performed under the direction of L. Bengtsson at the Max Planck Institute for Meteorology. The simulation with the ECHAM3 model covering 1970 to 1978 was conducted by M. Tyree. The NMC data were supplied by the NMC Coupled Model Project directed by A. Leetmaa. This work was supported by National Oceanic and Atmospheric Administration (NOAA) grant NA16RC0076-01 under the Global Change Program, by NOAA grant NA86AA-D-CP104 for the Experimental Climate Prediction Center at the Scripps Institution of Oceanography (SIO), by the University of California and Digital Equipment Corporation under research grant 1243, and by a grant from the G. Unger Vetlesen Foundation to SIO.

29 June 1994; accepted 21 November 1994